

Hot deformation behavior of an 8% Cr cold roller steel

Jiang Ping · Fu Wantang · Wang Zhenhua ·
Bai Xinghong · Zhao Xichun · Lv Zhiqing

Received: 23 December 2010 / Accepted: 4 February 2011 / Published online: 24 February 2011
© Springer Science+Business Media, LLC 2011

Abstract An 8% Cr cold roller steel was compressed in the temperature range 900–1200 °C and strain rate range 0.01–10 s⁻¹. The mechanical behavior has been characterized using stress-strain curve analysis, kinetic analysis, processing maps, etc. Metallographic investigation was performed to evaluate the microstructure evolution and the mechanism of flow instability. It was found that the work hardening rate and flow stress decreased with increasing deformation temperature and decreasing strain rate in 8% Cr steel; the efficiency of power dissipation decreased with increasing Z value; flow instability was observed at higher Z-value conditions and manifested as flow localization near the grain boundary. The hot deformation equation and the dependences of critical stress for dynamic recrystallization and dynamic recrystallization grain size on Z value were obtained. The suggested processing window is in the temperature range 1050–1200 °C and strain rate range 0.1–1 s⁻¹ in the hot processing of 8% Cr steel.

Introduction

Cold roller steels should have high strength and hardness, good toughness, and excellent wear resistance [1]. 8% Cr steel has higher chromium content, which is the trend in the development of cold roller steel [2]. In steel, the presence of a large amount of chromium induces higher martensite transformation start temperature, and then the critical quenching rate is lowered [3, 4]. Therefore, 8% Cr steel has better quench ability than 5% Cr steel. Deeper hardening depth can increase life of roller due to a larger available diameter. In addition, Cr promotes the precipitation of M₇C₃-type carbide and improves the wear resistance of roller [5]. Moreover, roller with higher Cr content has better thermal shock resistance, and then the formation and progression of cracks are restrained. Nowadays, 8% Cr steel, the new generation cold roller steel, gradually replaces 5% Cr steel.

8% Cr steel generally contains many alloy elements, such as Mo, Ni, V, and N, besides Cr. These elements can form fine carbonitrides intragranularly [5]. More types and high content of elements induce poor workability and bad controllability of microstructure of 8% Cr steel in hot processing.

The hot processing map technology based on the dynamic materials models has the capabilities of optimizing the parameters of processing technology, controlling microstructure and properties, and improving the hot working repeatability. It has been used to evaluate the thermal deformation mechanisms of a wide range of metal materials such as alloys of magnesium, aluminum, titanium, and Ni-base superalloys as well as austenitic steels [6–10]. This study aims to examine the mechanical behavior and microstructural evolution of an 8% Cr steel during hot compression, to identify the application of hot processing map technology in cold roller steel, and to

J. Ping · F. Wantang (✉) · W. Zhenhua · L. Zhiqing
State Key Laboratory of Metastable Materials Science and
Technology, Yanshan University, Qinhuangdao 066004,
People's Republic of China
e-mail: wtfu@ysu.edu.cn

W. Zhenhua · L. Zhiqing
College of Mechanical Engineering, Yanshan University,
Qinhuangdao 066004, People's Republic of China

J. Ping · B. Xinghong · Z. Xichun
China First Heavy Industries, Qiqihar 161042,
People's Republic of China

provide experimental warrants for establishing the hot working process.

Experimental procedures

The tested 8% Cr steel was melted in a 50 kg vacuum induction furnace. After electroslag remelting, its chemical composition is as follows (wt%): 0.60 C, 8.07 Cr, 0.55 Mn, 0.48 Si, 0.19 V, 0.61 Mo, 0.36 Ni, 0.01 P, 0.004 S, balance Fe. The electroslag remelted ingot was forged into bars with a diameter of 20 mm. The compression test specimens with a height of 15 mm and a diameter of 8 mm were machined from the center of the bar. Hot compression tests were conducted on a Gleeble 3500 thermal/mechanical simulator. Graphite foil was used as a lubricant between the specimen and compression dies. Thermocouples were welded on the surface of a compression specimen to measure temperature. The specimens were preheated at 1200 °C for 10 min, which leads to an initial grain size of approximately 200 μm, cooled to the test temperature at 10 °Cs⁻¹, and held for 5 s before deformation for temperature homogenization. The tests were performed at 900, 1000, 1100, and 1200 °C and strain rates of 0.01, 0.1, 1, and 10 s⁻¹, respectively. Specimens were deformed to a strain of 1.2, and then instantly quenched into water within 2 s. The deformed specimens were sectioned parallel to the compression direction. After being etched in a solution of nitric acid (20%) + alcohol (80%) or phosphoric acid (30%) + distilled water (70%), the microstructures were observed using optical microscopy.

Experimental results and analysis

Flow curves

The flow curves of 8% Cr steel obtained at strain rates of 0.01 and 10 s⁻¹ are shown in Fig. 1. It can be seen that work hardening rate and peak stress both increase with decreasing temperature and increasing strain rate. At 0.01 s⁻¹ (Fig. 1a), all curves are dynamic recrystallization type, i.e., the stress rises to a maximum at a peak strain and then diminishes to a value intermediate between the yield stress and the peak stress [11]. In Fig. 1b (10 s⁻¹), most of the curves are dynamic recovery type, i.e., the stress increases with increasing strain, up to a certain value, and then keep constant without changing with strain.

Hot deformation equation and Zener–Hollomon parameter

The relationship between the peak stress, the deformation temperature, and the strain rate (i.e., hot deformation

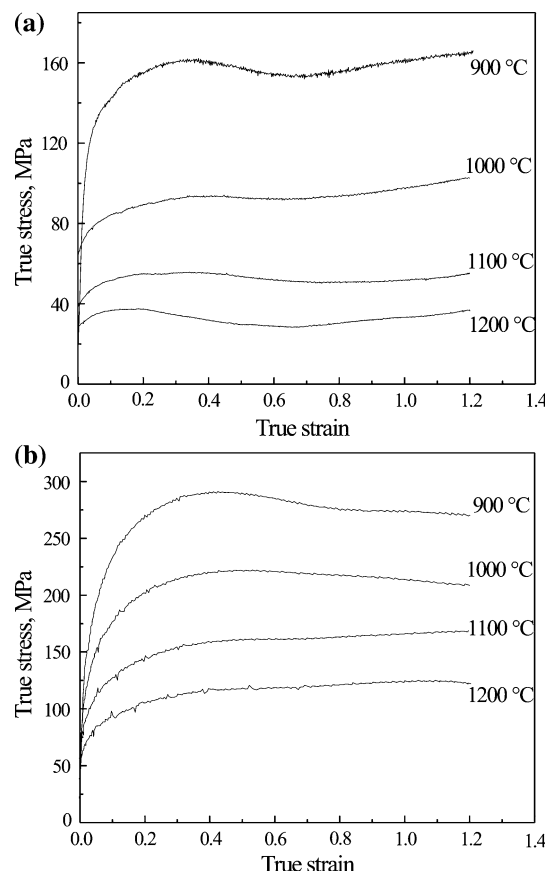


Fig. 1 Flow curves of 8% Cr steel under different strain rates **a** 0.01 s⁻¹; **b** 10 s⁻¹

equation) can be described as the classical hyperbolic sine function (Eq. 1) when the metal is deformed at elevated temperature [12]:

$$\dot{\varepsilon} = A[\sinh(\alpha\sigma)]^n \exp(-Q/RT) \quad (1)$$

where A and α are material constants, which are independent of deformation temperature, n is the stress exponent, Q a hot deformation activation energy, R the gas constant, T the absolute temperature, and σ is the static stress, or peak stress, or the stress for a given strain. In this study, the peak stress is taken. According to Ref. [13], through linear regression, average values of every parameter can be obtained: $A = 3.5 \times 10^{17}$, $\alpha = 0.008$, $n = 5.75$, $Q = 467 \text{ kJ mol}^{-1}$. The hot deformation equation and Zener–Hollomon parameter [14] (or temperature compensated strain rate) of 8% Cr steel can be expressed as follows:

$$\dot{\varepsilon} = 3.5 \times 10^{17} [\sinh(0.008\sigma)]^{5.75} \exp(-467000/RT) \quad (2)$$

$$Z = \dot{\varepsilon} \exp(467000/RT) \quad (3)$$

Figure 2 shows comparisons of experimental log(stress)–log(strain rate) data (points) with the calculated values (curves) for four different temperatures. It can be easily found that the proposed hot deformation equation gives an

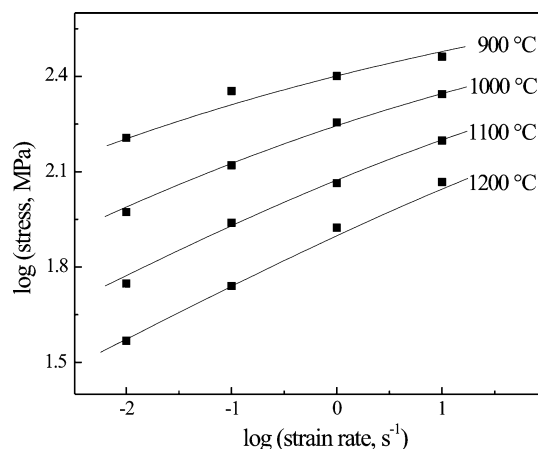


Fig. 2 Comparison between predicted (curves) and measured (points) flow stress of 8% Cr steel

accurate estimate of the peak stress for 8% Cr steel, and can be used to analyze the problems during metal forming process.

Critical stress for initiation of dynamic recrystallization

Poliak and Jonas [15] and Najafizadeh and Jonas [16] found that the initiation of dynamic recrystallization is associated with the point of inflection in the curve of strain hardening rate θ versus flow stress σ . According to their method, the strain hardening rate was plotted against flow stress, and the third-order equation that best fit the experimental $\theta-\sigma$ date from yield to the peak stress was found for each set of the deformation conditions. The critical stress for the initiation of dynamic recrystallization (σ_c) was obtained numerically from the coefficients of the third-order equation. Thus, for 8% Cr steel, the relationship between σ_c and Z is obtained, as shown in Fig. 3. There is a linear relationship between σ_c and $\ln Z$:

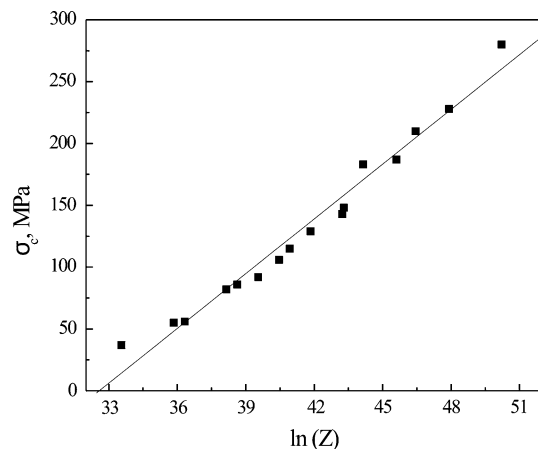


Fig. 3 Dependence of the critical stress for the initiation of dynamic recrystallization on Z parameter

$$\sigma_c = 14.7 \ln Z - 480 \text{ (MPa)} \quad (4)$$

Processing maps

The theoretical basis and methods for hot processing maps to be established have been described in detail earlier by Prasad and Sasidhara [17]. A workpiece deformed under hot working conditions can be considered to be a power dissipater. The strain rate-sensitivity index m for determining the distribution between the system power dissipation caused by viscous-plastic deformation and that caused by structural changes, wherein the ratio of power dissipation due to structural changes in the deformation process is denoted by η (known as the “power dissipation ratio”), indicate how efficiently the material dissipates energy under microstructural changes. This finding can be defined as Eq. 5:

$$\eta = \frac{2m}{m+1} \quad (5)$$

This parameter η varies with deformation temperature and strain rate. The power dissipation map can be obtained based on the values of η under different conditions. Equation 6 shows the flow instability criteria [17]:

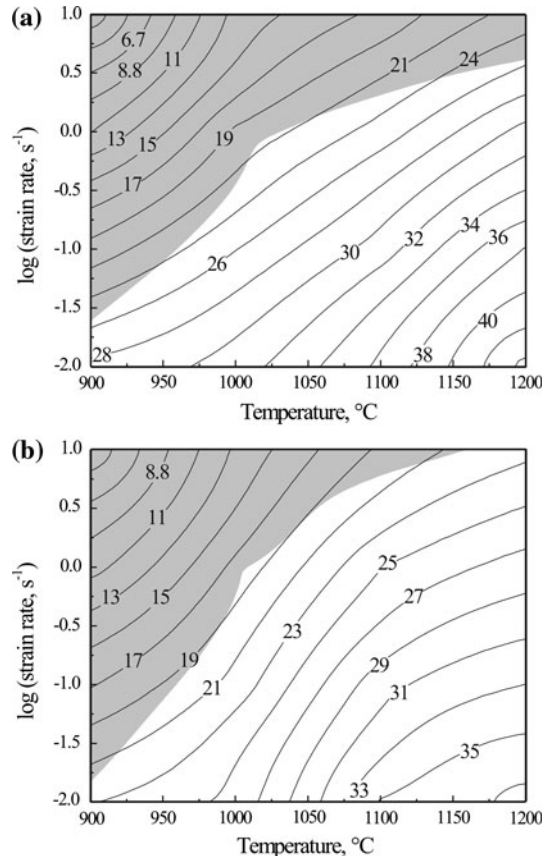


Fig. 4 Processing maps obtained on 8% Cr steel at different strains
(a) 0.6; (b) 1.2

$$\xi = \left\{ \frac{\partial \ln[m/(m+1)]}{\partial \ln \dot{\epsilon}} \right\} + m < 0 \quad (6)$$

Flow instabilities are predicted to occur when ξ is negative. The instability map may be superimposed on the power dissipation map to obtain a processing map. Processing maps for the tested steel, developed at different strains, are shown in Fig. 4.

Contour numbers represent the percentage efficiency of dissipation, and the shaded region corresponds to the flow instability in Fig. 4. It can be seen from both figures that the efficiency of power dissipation increases with increasing temperature and decreasing strain rate, i.e., with decreasing Z value. The efficiency reaches a highest value of 44% at 1200 °C and 0.01 s⁻¹ in Fig. 4a. Over the entire range of test parameters, flow instability is observed at higher Z -value conditions. The extent of the flow instability region at 0.6 is slightly larger than 1.2.

The microstructures of the specimens deformed in different regions in Fig. 4b are shown in Fig. 5a through d. Figure 5a and b shows the microstructures in the flow instability region. It can be seen that fine dynamic recrystallization grains appear around parent grains, which is called necklace structure [18]. Jafari and Najafizadeh [19] reported that grain boundary shearing or sliding usually takes place in a coarse-grained structure under deformation

at low temperature or at high-strain rate and can lead to the development of inhomogeneous deformation. Here, grain boundary shearing means local shear deformation in the narrow regions near the grain boundary while sliding occurs at the grain boundary, which led to necklace dynamic recrystallization [19]. The occurrence of necklace DRX in Fig. 5a and b means that flow localization occurs near grain boundaries. Therefore, for 8% steel, the flow localization near parent grain boundaries is the mechanism of flow instability. In the specimens deformed in flow instability region, the strain distribution is non-uniform. There is strain gradient from the boundary to the interior of the parent grain. It has been well known that the extent of necklace DRX increases with increasing strain. More new small grains can lower the strain gradient in the steel and the flow instability is restrained. Therefore, the extent of the flow instability region at 0.6 is slightly larger than 1.2 (Fig 4). In Fig. 5c and d (stable region), full DRX can be found.

In fact, the dynamic recrystallization grain size (D) depends on the parameters Z and A [20], and A is the same parameter as that in Eq. 1. The dependence of $\ln(D)$ obtained by the linear intercept method on $\ln(Z/A)$ is shown in Fig. 6.

The relationship between D (μm) and (Z/A) can be expressed by the following equation:

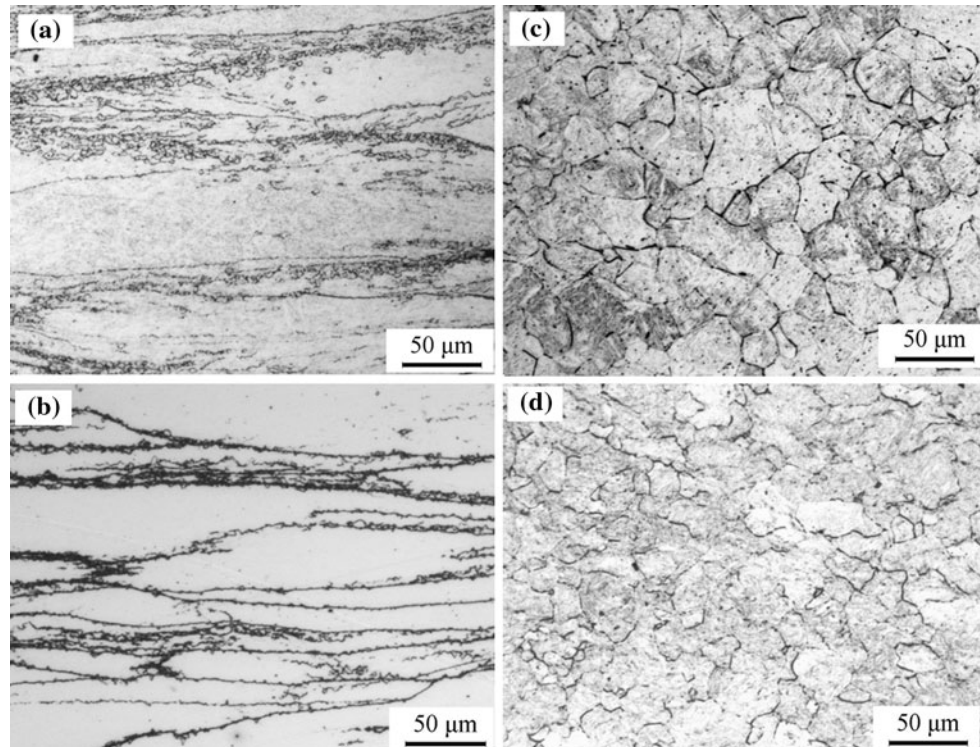


Fig. 5 Typical microstructures of 8% Cr steel deformed under different conditions **a** 900 °C 10 s⁻¹; **b** 900 °C 0.1 s⁻¹; **c** 1200 °C 10 s⁻¹; **d** 1100 °C 0.1 s⁻¹

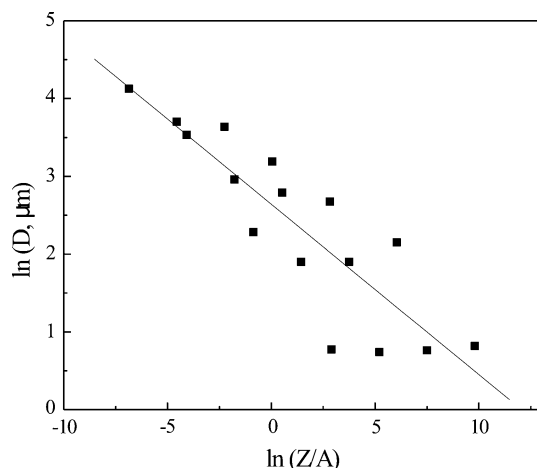


Fig. 6 Dependence of dynamic recrystallization grain size on parameters Z and A

$$D = 2.64 \times (Z/A)^{-0.224} (\mu\text{m}). \quad (7)$$

It is very interesting to note that the larger the Z value, the more discrete the D in Fig. 6. This phenomenon may be caused by deformation heating [21]. As mentioned above, the efficiency of power dissipation increases with decreasing Z value. It means that the ratio of power dissipation caused by viscous-plastic deformation is larger under higher Z -value conditions, and also the deformation heating. Especially under higher strain rate conditions, the heating effect is more apparent due to the short diffusion time [22]. Figure 7 shows the temperature variation of 8% Cr steel in the deformation process (900°C , 10 s^{-1}). Obviously, the temperature increase reaches 37°C when the strain is up to 1.2. Deformation heating occurs at other deformation conditions also and increases with increasing Z value. The dynamic recrystallization grain size is undoubtedly affected by temperature increase.

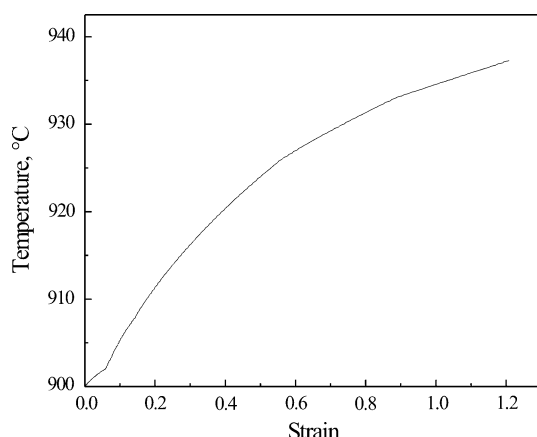


Fig. 7 Temperature variation of 8% Cr steel in the deformation process (900°C , 10 s^{-1})

It is suggested that deformation should be carried out in the temperature range $1050\text{--}1200^\circ\text{C}$ and strain rate range $0.1\text{--}1\text{ s}^{-1}$ in the hot processing of 8% Cr steel to avoid flow instability and coarse-grained structure.

Conclusions

- (1) The hot deformation equation of 8% Cr steel deformed at $900\text{--}1200^\circ\text{C}$ and $0.01\text{--}10\text{ s}^{-1}$ is $\dot{\varepsilon} = 3.5 \times 10^{17} [\sinh(0.008\sigma)]^{5.75} \exp(-467000/RT)$.
- (2) For 8% Cr steel, the flow stress and work hardening rate decreased with increasing deformation temperature and decreasing strain rate, and the relationship between the critical stress for initiation of dynamic recrystallization and the Zener–Hollomon parameter is $\sigma_c = 14.7 \ln Z - 480$ (MPa).
- (3) The dependence of dynamic recrystallization grain size on parameters Z and A can be shown as $D = 2.64 \times (Z/A)^{-0.224}$ (μm). The larger the Z value, the more discrete the dynamic recrystallization grain size.
- (4) In the processing map, the flow instability was observed at the high Z -value region and manifested as flow localization near the grain boundary. The suggested processing window is in the temperature range $1050\text{--}1200^\circ\text{C}$ and strain rate range $0.1\text{--}1\text{ s}^{-1}$ in the hot processing of 8% Cr steel.

Acknowledgement The research was supported by the Science Research and Development of Qinhuangdao (201001A109).

References

1. Ray AK, Mishra KK, Das G (2000) Eng Fail Anal 7:55
2. Nishida M, Suemune K, Nonaka Y (1990) Iron Steel Eng 67:49
3. Bodnar RL, Minfa Lin, Hansen SS (1993) Iron & Steelmaker 20:65
4. Liu XL, Zhang HK (2008) Heat Treat 23:16 (in Chinese)
5. Zhao X, Li WP, Liu DF (2004) Heavy Cast Forg 105:38 (in Chinese)
6. Wang CY, Wang XJ, Chang H (2007) Mater Sci Eng A 464:52
7. Menon SS, Rack HJ (2001) Mater Sci Eng A 297:244
8. Park NK, Yeom JT, Na YS (2002) J Mater Process Technol 130–131:540
9. Prasad YVRK, Sasidhara S, Sikka VK (2000) Intermetallics 8:987
10. Venugopal S, Sivaprasad PV, Vasudevan M (1995) J Mater Process Technol 59:343
11. Sakai T, Jonas JJ (1984) Acta Metall 32:189
12. Sellars CM (1900) In: Yue Sed Proceedings of the International Conference on Mathematical Modelling of Hot Rolling of Steel. CIMM, Hamilton
13. Lu YH, Fu RD, Qiu L (2007) Trans Mater Heat Treat 28:69 (in Chinese)
14. Medina SF, Hernandez CA (1996) Acta Mater 44:137

15. Poliak EI, Jonas JJ (2003) *ISIJ Int* 43:684
16. Najafizadeh A, Jonas JJ (2006) *ISIJ Int* 46:1679
17. Prasad YVRK, Sasidhara S (1997) Hot working guide: a compendium of processing maps. American Society for Materials International, Materials Park, p 10–24
18. Ponge D, Gottstein G (1998) *Acta Metall* 46:69
19. Jafari M, Najafizadeh A (2009) *Mater Sci Eng A* 501:16
20. Kim SI, Yoo YC (2001) *Mater Sci Eng A* 311:108
21. Liu JT, Chang HB, Wu RH (2000) *Mater Character* 45:175
22. Tan SP, Wang ZH, Cheng SC (2010) *Int J Miner Metall Mater* 17:167